Measuring Global Ocean Wave Skewness by Retracking RA-2 *Envisat* Waveforms

J. GÓMEZ-ENRI, C. P. GOMMENGINGER, M. A. SROKOSZ, AND P. G. CHALLENOR

Laboratory for Satellite Oceanography, National Oceanography Centre, Southampton, United Kingdom

J. BENVENISTE

ESRIN, European Space Agency, Frascati, Italy

(Manuscript received 23 June 2005, in final form 16 August 2006)

ABSTRACT

For early satellite altimeters, the retrieval of geophysical information (e.g., range, significant wave height) from altimeter ocean waveforms was performed on board the satellite, but this was restricted by computational constraints that limited how much processing could be performed. Today, ground-based retracking of averaged waveforms transmitted to the earth is less restrictive, especially with respect to assumptions about the statistics of ocean waves. In this paper, a theoretical maximum likelihood estimation (MLE) ocean waveform retracker is applied tothe *Envisat* Radar Altimeter system (RA-2) 18-Hz averaged waveforms under both linear (Gaussian) and nonlinear ocean wave statistics assumptions, to determine whether ocean wave skewness can be sensibly retrieved from *Envisat* RA-2 waveforms. Results from the MLE retracker used in nonlinear mode provide the first estimates of global ocean wave skewness based on RA-2 *Envisat* averaged waveforms. These results show for the first time geographically coherent skewness fields and confirm the notion that large values of skewness occur primarily in regions of large significant wave height. Results from the MLE retracker run in linear and nonlinear modes are compared with each other and with the RA-2 Level 2 Sensor Geophysical Data Records (SGDR) products to evaluate the impact of retrieving skewness on other geophysical parameters. Good agreement is obtained between the linear and nonlinear MLE results for both significant wave height and epoch (range), except in areas of high-wave-height conditions.

1. Introduction

The main aim of the tracking system on board satellite altimeters is to search for and maintain the return signals in the altimeter analysis window (Zanife et al. 2003). In early altimeters, the onboard tracking system also determined in real time the epoch (related to the range), the backscatter coefficient (related to the wind speed), and the significant wave height, but computational constraints on board limited how much processing could be performed. Today, most altimeters transmit averaged waveforms directly to the ground, where more extensive ground-based retracking can take place. This allows greater flexibility with respect to various assumptions about how to retrieve geophysical parameters from the waveforms.

For European Remote Sensing Satellites *ERS-1* and *ERS-2*, high-precision tracking was required over the ocean, but the altimeter also had to be capable of maintaining track over the continental ice sheets (Griffiths et al. 1987). The onboard "ocean" tracking system used for the fast delivery products was the suboptimal maximum likelihood estimator (Losquadro 1983), optimized for altimeter returns over the ocean, obeying the Brown model (Brown 1977). The "ice" tracking system used the 3:1 weighted split gate tracker (historically referred to as a center of gravity tracker) with a range resolution of 1.8 m (12.12 ns). However, such algorithms were unstable, generating error signals in nonnominal conditions. To produce the ERS Ocean Products (OPR), ground-based processing of waveforms was used instead. For ERS, this ground-based retracking used a maximum likelihood estimation (MLE) algorithm.

Corresponding author address: J. Gómez-Enri, Laboratory for Satellite Oceanography, National Oceanography Centre, Southampton, European Way, Southampton SO14 3ZH, United Kingdom.
E-mail: jxge@noc.soton.ac.uk

DOI: 10.1175/JTECH2014.1

The ground-based retracker for the *Envisat* Radar Altimeter (RA-2) has been optimized to ensure that geophysical parameters can be obtained over all types of surfaces (ocean, land, ice, etc.). To do that, four retrackers are applied in parallel to all waveforms obtained over all surfaces. This represents a major change with respect to the previous altimeters on *ERS-1* and *-2*. The RA-2 ocean retracker is the result of a comparative study of various ocean-retracking algorithms (ESA 2004) and is based on a modification of the Hayne model (Hayne 1980). This model is an extension of the Brown model (Brown 1977), with some nonlinearity of the ocean waves included by setting the wave skewness to a fixed constant value. The RA-2 altimeter design also allows improved estimates of the slope of the leading edge of the waveform in low-wave-height conditions, thanks to two optional extra gates in the central part of the waveform leading edge, which make it possible to measure even small wave heights with improved accuracy.

This paper presents the results obtained when retracking RA-2 *Envisat* 18-Hz averaged waveforms with the MLE waveform retracker developed at the National Oceanography Centre (NOC), Southampton. The NOC MLE retracker is able to operate in both linear and nonlinear modes to retrieve significant wave height (SWH) and range (or epoch, or time origin, t_0), as well as ocean wave skewness when run in nonlinear mode. The purpose of this paper is to determine whether physically meaningful estimates of ocean wave skewness can be retrieved from *Envisat* RA-2 waveforms and to evaluate what the impact of retrieving skewness is on the other geophysical parameters. For this, we compare the results of our linear and nonlinear MLE retracking with each other and with the RA-2 Level 2 Sensor Geophysical Data Record (SGDR) products provided by the European Space Agency (ESA).

The layout of the paper is as follows. Section 2 provides some background about the theoretical modeling of ocean waveforms. We give details of the NOC retracker scheme with emphasis on maximum likelihood estimation and the retrieval of linear and nonlinear ocean parameters. In section 3, a short overview is given of the altimeter data used, followed in section 4 by the results obtained with the MLE retracker run in linear and nonlinear modes, and our comparisons with the ESA SGDR results. Section 5 gives the conclusions and final remarks.

2. Retracking ocean waveforms

The error in altimetric range due to surface wave effects is known as sea-state bias. Sea-state bias arises from a number of factors: the behavior of the onboard tracker, the electromagnetic and skewness effects on the scattering of the altimeter pulse from the sea surface and, possibly, various operational corrections made to the data (e.g., the dual-frequency correction for the ionospheric effect). In addition, ground retracking of ocean waveforms—and the wide range of subtle differences arising from different implementations—complicate the picture. In this paper, we focus on just one aspect of waveform retracking, related to the effect of wave skewness. Our objective is to determine whether physically meaningful skewness estimates can be obtained globally by retracking *Envisat* RA-2 waveforms, and what the impact of retrieving skewness is on range and significant wave height. The importance of skewness in altimeter tracker bias is examined more specifically in another paper (Gomez-Enri et al. 2006).

a. Theoretical models of ocean waveforms

The high-precision retrieval of geophysical information from altimeter waveforms over the ocean is possible thanks to the well-developed theoretical modeling of altimeter echoes from the ocean surface. The way in which the echo return interacts with the illuminated ocean surface is described in Brown (1977). Basically, the return power of the surface $[P_r(t)]$ is the result of the convolution of three terms:

$$P_r(t) = P_{\mathrm{FS}}(t) * q(t) * P_{\mathrm{PT}}(t),$$

where t is the time, and $P_{\mathrm{FS}}(t)$ is the flat surface response as described by Brown (1977), which includes the antenna pattern of the altimeter:

$$P_{\mathrm{FS}}(t) = \frac{\mathrm{const1} * \mathrm{sigma0}}{h^3} \exp\left\{ -\frac{4}{\gamma}\sin^2\xi - \frac{4c}{\gamma h} t \cos 2\xi \right\} I_0\left(\frac{4}{\gamma}\sqrt{\frac{ct}{h}}\sin 2\xi \right) \quad (2)$$

for $t \geq t_0$;

$$P_{\mathrm{FS}}(t) = \frac{\mathrm{const1} * \mathrm{sigma0}}{h^3} \exp\left\{ -\frac{4}{\gamma}\sin^2\xi \right\} \quad (3)$$

for $t < t_0$, where

$$\mathrm{const1} = \frac{G_0^2 \lambda_R^2 c \eta P_T \sigma_P}{4(4\pi)^2 L_p} \sqrt{\frac{\pi}{2}},$$

where G_0 is the antenna gain parameter, λ_R is the radar wavelength, c is the velocity of light in vacuo, η is the pulse compression ratio, P_T is the transmitted power, σ_P is related to the pulse width (see more on σ_P in the section below on P_{PT}), and L_p is the two-way propagation loss over and above the free-space loss; $\gamma = (\sin^2\Psi_B/2\ \ln 2)$, with Ψ_B the half-power (3 dB) antenna beamwidth, sigma0 is the radar backscatter cross section, ξ is the mispointing angle (from nadir), $I_0(t)$ is the modified Bessel function of the first kind (Abramowitz and Stegun 1968), t_0 is the epoch ($=2h/c$) that represents the position in time of the ocean surface, and h is the satellite height [note that the earth radius term suggested by Rodríguez (1988) is not included here; it only affects the value of the retrieved backscattered power, and so does not impact the results presented in this paper; see section 3].

The probability density function of the height of specular points on the sea surface, $q(t)$, or more precisely, $q(h)$, is given by Srokosz (1986) for weakly nonlinear ocean waves as

$$q(t) = \frac{1}{\sqrt{2\pi}\sigma_s}\exp\left[\frac{-c(t-t_0)^2}{2\sigma_s^2}\right]\left\{1 + \frac{1}{6}\lambda H_3\left[\frac{c(t-t_0)}{\sigma_s}\right] - \frac{1}{2}\delta H_1\left[\frac{c(t-t_0)}{\sigma_s}\right]\right\}, \tag{4}$$

where σ_s is the standard deviation of sea surface elevation ($=\mathrm{SWH}/4$), λ is the ocean skewness [defined as λ_{300} in Srokosz (1986)], H_3 is the Hermitian polynomial of order 3, δ is the cross-skewness [defined as γ in Srokosz (1986)], and H_1 is the Hermitian polynomial of order 1. The cross-skewness is defined as the normalized expectation of the elevation and slope squared and has no clear physical meaning. In all our calculations, this term is set to zero because, as Tokmakian et al. (1994) previously showed using MLE applied to simulated waveforms, it is not possible to estimate both cross-skewness and epoch accurately because of their high correlation. Under the Srokosz (1986) theory, estimates of the altimeter ranging error due to wave nonlinearity could in principle be obtained from the skewness and cross-skewness parameters, although Rodriguez (1988) suggested that these non-Gaussian parameters cannot be extracted in practice from altimeter waveforms.

Finally, $P_{\mathrm{PT}}(t)$ is the theoretical radar point target response (PTR) function, which can be represented as $[\sin(\mathrm{B}t)/(\mathrm{B}t)]^2$, where B is the altimeter signal bandwidth (Callahan and Rodríguez 2004). To obtain an analytical expression for the convolution of the three terms in Eq. (1), the PTR function is approximated by a Gaussian function (Amarouche et al. 2004; Thibaut et al. 2004a):

$$P_{\mathrm{PT}}(t) = \eta P_T \exp\left(-\frac{t^2}{2\sigma_p^2}\right), \tag{5}$$

where P_T is the peak transmitted power. The nominal value for σ_P is 0.425* (pulse width) for *Envisat*. However, it recently emerged that the ESA ground retracker for *Envisat* uses a value of σ_p equal to 0.53* (pulse width).

The final expressions for the returned power are (setting cross-skewness to zero)

$$P_r(t) = \frac{\mathrm{const1}\times\mathrm{sigma0}}{h^3}\exp\left[-\frac{4}{\gamma}\sin^2\xi - \frac{4c}{\gamma h}(t-t_0)\cos 2\xi\right] I_0\left[\frac{4}{\gamma}\sqrt{\frac{c(t-t_0)}{h}}\sin 2\xi\right]$$
$$\times\left\{\mathrm{erfc}\left[\frac{-(t-t_0)}{\sqrt{2}\sigma_c}\right] - \frac{1}{\sqrt{2\pi}}\exp\left[\frac{-(t-t_0)^2}{2\sigma_c^2}\right]\frac{\lambda\mathrm{SWH}^3}{24c^3\sigma_c^3}H_2\left[\frac{(t-t_0)}{\sigma_c}\right]\right\} \quad \text{for} \quad t \geq t_0 \tag{6}$$

and

$$P_r(t) = \frac{\mathrm{const1}\times\mathrm{sigma0}}{h^3}\exp\left(-\frac{4}{\gamma}\sin^2\xi\right)\left\{\mathrm{erfc}\left[\frac{-(t-t_0)}{\sqrt{2}\sigma_c}\right] - \frac{1}{\sqrt{2\pi}}\exp\left[\frac{-(t-t_0)^2}{2\sigma_c^2}\right]\frac{\lambda\mathrm{SWH}^3}{24c^3\sigma_c^3}H_2\left[\frac{(t-t_0)}{\sigma_c}\right]\right\} \quad \text{for} \quad t < t_0 \tag{7}$$

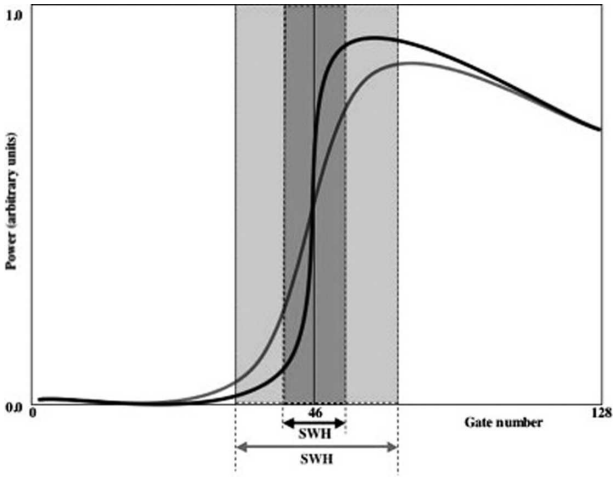

FIG. 1. Representation of two idealized altimeter echoes for two different conditions of significant wave height. Also shown, the position of the tracking point (gate number 46) used to determine the position of the tracking window.

where

$$\sigma_c = \sqrt{\sigma_p^2 + \frac{4\sigma_s^2}{c^2}},$$

and erfc(x) is the complementary error function (Abramowitz and Stegun 1968). Note that if the probability density function of reflected facets is considered Gaussian, the coefficient of wave skewness (λ) vanishes and we obtain the model radar returned power [$P_r(t)$] described by Brown (1977).

Figure 1 shows the evolution of the received power in time as a ramp starting at zero and rising with time to a plateau, after which it falls off slowly (Barrick and Lipa 1985). Wind speed information can be extracted from the radar backscatter coefficient, which is linked to the received power at the plateau. The slope of the leading edge is related to the significant wave height. The position of the midpoint of the leading edge gives the epoch (time origin) parameter, which can be combined with tracking information to derive the range parameter. The slope of the trailing edge can provide information on the instrument mispointing (attitude) away from nadir.

b. The NOC ocean retracking scheme

The NOC retracking scheme described here was originally designed and developed at the Institute of Oceanographic Sciences (IOS) (Challenor and Srokosz 1989) to retrieve improved geophysical parameters from *ERS-1* radar altimeter waveforms (Griffiths et al., 1987). In its linear form, the NOC retracker provides estimates of SWH, the backscatter power (related to the wind speed), the epoch (time origin), and the thermal noise. In its nonlinear mode, extra information can be retrieved about skewness, which characterizes the weakly nonlinear nature of ocean waves (i.e., peakier crests/flatter troughs).

To retrieve geophysical parameters with RA-2 18-Hz averaged waveforms, a number of modifications were made to account for differences in altimeter specifications between *ERS-1/2* and RA-2. Hence, the number of gates was changed from 64 to 128, and gate spacing was changed from 3.03 to 3.125 ns. The nominal tracking point was modified from 31.5 to 45. All results in this paper were obtained with the nominal *Envisat* value of $\sigma_P = 0.425*$ (pulse width).

The NOC retracker in its present form does not retrieve mispointing (attitude), nor does it use any (nonzero) value of mispointing as input. *Envisat* has proved to be a very stable platform, with no significant mispointing for RA-2 reported so far. Yet, attitude has a huge impact on the shape of the waveforms, much greater than skewness, so that, in principle, one should use the best available estimates of attitude for the retracking. In principle, mispointing can be estimated directly from the slope of the waveform trailing edge and can then be injected as input to the retracker. However, estimates of RA-2 attitude obtained with this method are found to be much noisier along-track, as one would expect (Thibaut et al. 2004a) as a result of rapidly fluctuating instrument artifacts in a small number of gates in the trailing edge. It was shown in Challenor and Srokosz (1989) that if you attempt to estimate σ^0 and attitude, the Fisher information matrix becomes singular, giving infinite variances for the estimators (see below for details on the Fisher information matrix). Given that the mispointing of RA-2 is known to be small and that using erroneous attitude values would be detrimental to observing the more subtle skewness effects in the waveforms, we therefore chose to proceed with a constant attitude set to zero (0). The significant impact on range and skewness estimates of using erroneous attitude as input to the retracker is being examined in detail in another paper (Gomez-Enri et al. 2007, hereafter GOM).

c. Maximum likelihood estimation

The NOC retracker derives geophysical parameters by fitting a theoretical model [Eqs. (6) and (7)] to measured waveforms using maximum likelihood estimation. The MLE method estimates the parameters by determining which values maximize the probability of obtaining the recorded waveform shape in the presence

TABLE 1. Characteristics of various retracking schemes used in the present paper.

	ESA RA-2 Level 2	NOCS MLE Linear	NOCS MLE Nonlinear	Callahan and Rodríguez (2004)	Thibaut et al. (2004a)
Satellite	*Envisat*	*Envisat*	*Envisat*	*Jason-1*	*Jason-1*
No. of gates	128	128	128	128	128
Tracking point	46	45	45	44	44
Fitting method	"WLS"[a] (LS)	MLE[b]	MLE	SVD[c] (LS)	"MLE"[d] (LS)
Skewness	Fixed ($\lambda = 0$)	Fixed ($\lambda = 0$)	Retrieved	Retrieved	Retrieved
Off-nadir mispointing	Yes, as input[e]	No	No	Yes	Yes

[a] Weighted least squares, with uniform weighting (O. Z. Zanife 2006, personal communication), so, effectively, least squares (LS).
[b] Maximum likelihood estimation.
[c] Least squares (LS) using the singular value decomposition method (Callahan and Rodríguez 2004)
[d] Maximum likelihood estimation, with uniform weighting (P. Thibaut 2006, personal communication), so, effectively, least squares (LS).
[e] This parameter is measured in near–real time from the RA-2 instrument pitch and roll angles interpolated to the RA-2 record time.

of noise of a given statistical distribution. The MLE technique can be shown to be asymptotically an optimal way of fitting noisy altimeter waveform data. MLE gives unbiased estimates with minimum variance and produces a variance–covariance matrix of the estimates, which provides a measure of the error in the estimates.

The maximum probability of obtaining the recorded waveform shape is derived by differentiating the likelihood function [the product of the probability densities evaluated at each data point (see Tokmakian et al. 1994)] with respect to the unknown parameters and setting the derivatives to zero. This technique is explained in greater detail in Challenor and Srokosz (1989) and Tokmakian et al. (1994), the latter including some examples of estimation of the parameters using

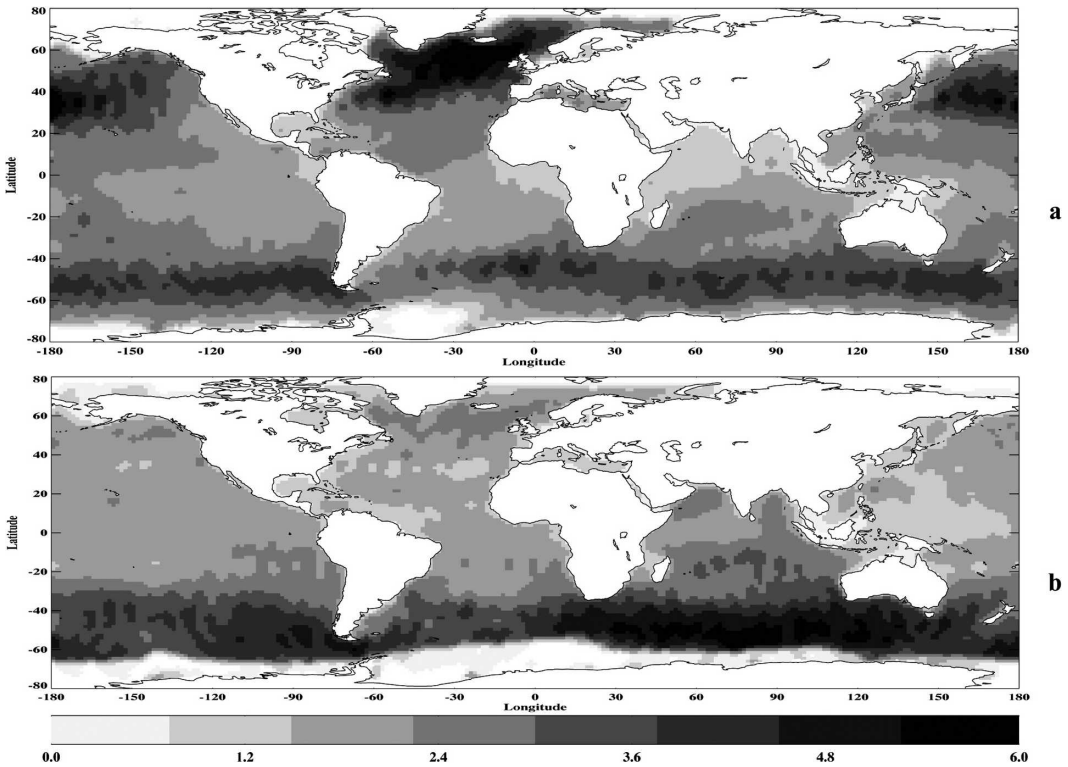

FIG. 2. Geographical distribution of SWH retrieved with MLE-L for (a) cycle 13 (Jan–Feb 2003) and (b) cycle 19 (Aug–Sep 2003). Units: m.

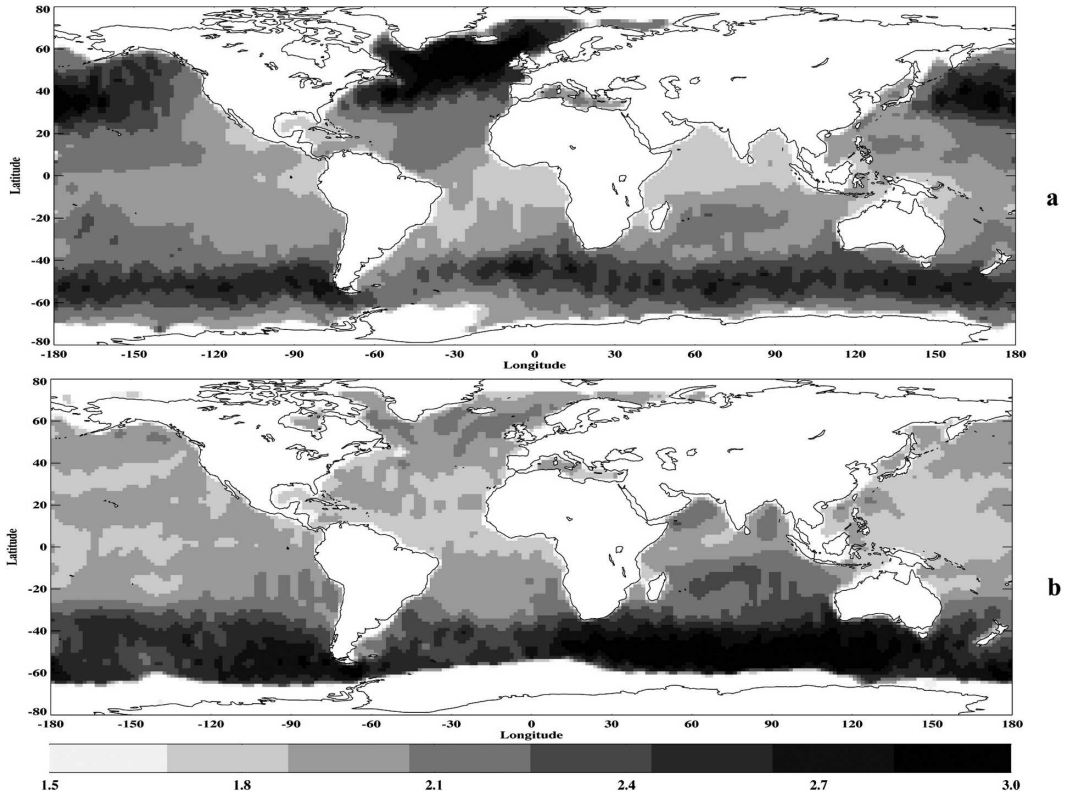

FIG. 3. Geographical distribution of the standard deviations of SWH retrieved with MLE-L for (a) cycle 13 and (b) cycle 19. Units: cm.

simulated averaged waveforms for *ERS-1*. Repeated here for ease of reference, the log-likelihood function for an altimeter radar power return to be maximized (LL) is given by

$$\mathrm{LL} = \sum_{i=1}^{n} [N \ln N + (N-1)\ln\hat{u}_i - \ln(N-1)]! - N\ln u_i - N\frac{\hat{u}_i}{u_i}, \quad (8)$$

where N is the number of pulses averaged (= 100 for 18-Hz waveforms), n is the number of bins (or gates, for RA-2, $n = 128$) in each waveform, $\hat{u}_i$ is the measured return power in the ith bin, and u_i is the theoretical return power $[P_r(t_i) + T_N]$ (T_N denotes thermal noise) and a function of the parameters that we wish to estimate. The first derivatives of Eq. (8) are

$$\frac{\partial \mathrm{LL}}{\partial \theta_j} = N \sum_{i=1}^{n} \frac{\partial u_i(\theta_j)}{\partial \theta_j}\left(\frac{\hat{u}_i}{u_i^2} - \frac{1}{u_i}\right), \quad (9)$$

where θ_j represents the parameters to be retrieved; and $j = 1, \ldots, n\mathrm{par}$, with $n\mathrm{par} = 4$ in linear mode (significant wave height, backscatter amplitude, epoch, and thermal noise) and $n\mathrm{par} = 5$ in nonlinear mode (same as linear, plus wave skewness). The first three terms in Eq. (8) are constant and therefore vanish in Eq. (9) since they are not a function of any of the variables we wish to estimate.

As mentioned, the MLE technique makes it possible to derive the variance–covariance matrix $\mathbf{V}$ to give a measure of the possible error in our estimates. It is given as the inverse of the Fisher information matrix $\mathbf{F}$ (i.e., the inverse of the matrix of second derivatives calculated from the MLE estimates) (Challenor and Srokosz 1989), so

$$\mathbf{V} = \mathbf{F}^{-1}, \quad (10)$$

where

$$\mathbf{F} = \left[E\left(\frac{\partial \mathrm{LL}}{\partial \theta_j}\frac{\partial \mathrm{LL}}{\partial \theta_k}\right)\right], \quad (11)$$

where $j, k = 1, \ldots, n\mathrm{par}$ and $E(..)$ denotes the expectation operator (Cox and Hinkley 1974). From Eq. (9) we obtain

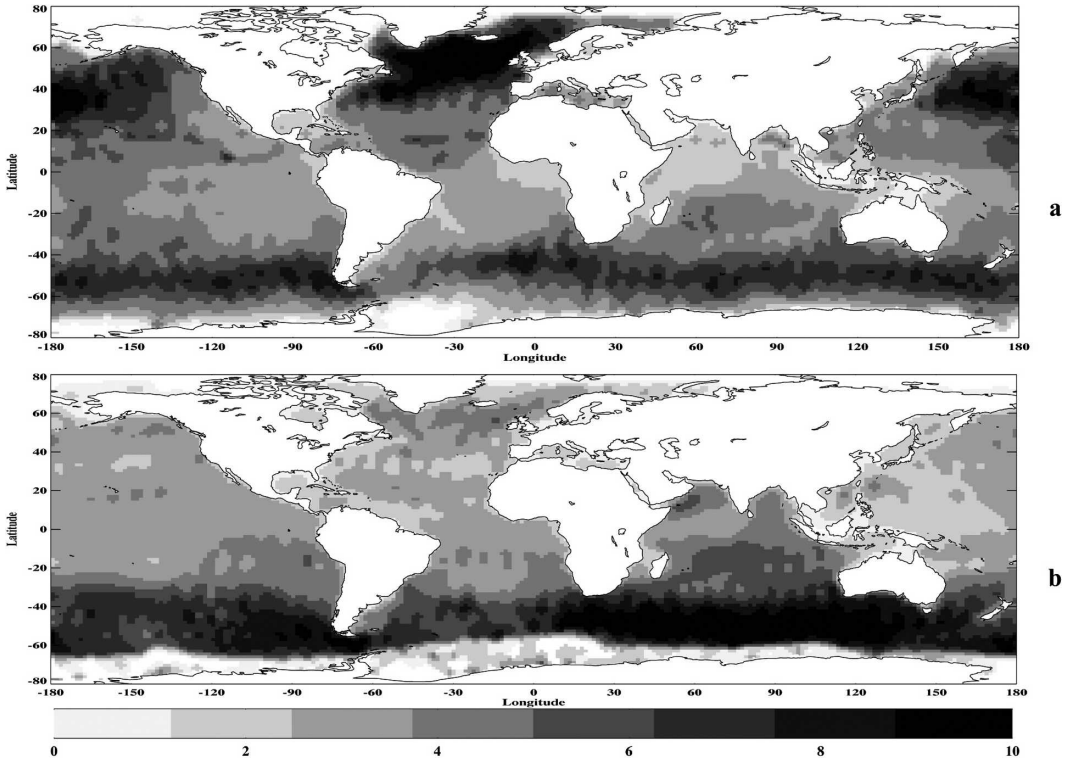

FIG. 4. Geographical distribution of the epoch retrieved with MLE-L for (a) cycle 13 and (b) cycle 19. Units: ns.

$$\left(\frac{\partial \mathrm{LL}}{\partial \theta_j}\frac{\partial \mathrm{LL}}{\partial \theta_k}\right) = N^2 \sum_{i=1}^{n}\sum_{r=1}^{n}\left(\frac{\hat{u}_i - u_i}{u_i^2}\frac{\hat{u}_r - u_r}{u_r^2}\frac{\partial u_i}{\partial \theta_j}\frac{\partial u_r}{\partial \theta_k}\right), \tag{12}$$

with $i, r = 1, \ldots, n$.

It has been shown (Ulaby et al. 1982) that the return power in any given gate for a single pulse has a negative exponential distribution with mean equal to the theoretical return power. Assuming that the altimeter moves at least the diameter of the antenna between transmitting pulses and that the signal in adjacent gates is independent, the samples can be assumed to be independent, and the average of N pulses with negative exponential distribution will have a gamma or chi-squared distribution (Challenor and Srokosz 1989). With the properties of the gamma distribution and the assumption of independence between gates and pulses we have

$$E[(\hat{u}_i - u_i)(\hat{u}_r - u_r)] = \frac{u_i^2}{N}\delta_{ir}, \tag{13}$$

where δ_{ir} is the Kronecker delta. Together with Eq. (11) these give the following result for $\mathbf{F}$:

$$\mathbf{F} = \left(N\sum_{i=1}^{n}\frac{1}{u_i^2}\frac{\partial u_i}{\partial \theta_j}\frac{\partial u_i}{\partial \theta_k}\right), \tag{14}$$

where N is the number of pulses averaged, n is the number of gates in the waveform, and $j, k = 1, \ldots, n\mathrm{par}$, where $n\mathrm{par}$ is the number of parameters to be retrieved.

From Eq. (14) the inverse may be calculated numerically to obtain the variance–covariance matrix $\mathbf{V}$ [Eq. (10)].

From the properties of maximum likelihood estimators (see, e.g., Cox and Hinkley 1974) we know that asymptotically the MLE is statistically efficient and attains the Cramer–Rao lower bound [given by the inverse of Eq. (14)]. This means that there is no unbiased estimator with a lower variance.

d. Other retracking schemes

The use of an independent MLE-based ocean retracker enables comparison against the results obtained with other retracking schemes. Geophysical parameters provided to the scientific community in the ESA Level 2 products (SGDR and GDR) are obtained under the assumption of linearity (skewness set to fixed value of 0 by default; M. P. Milagro-Perez, ESA, 2005, personal communication) using a weighted least squares (WLS) estimation and the Levenberg–Marquardt method (Press et al. 1988). Depending on the definition of the weights, WLS may be the same as MLE. When the

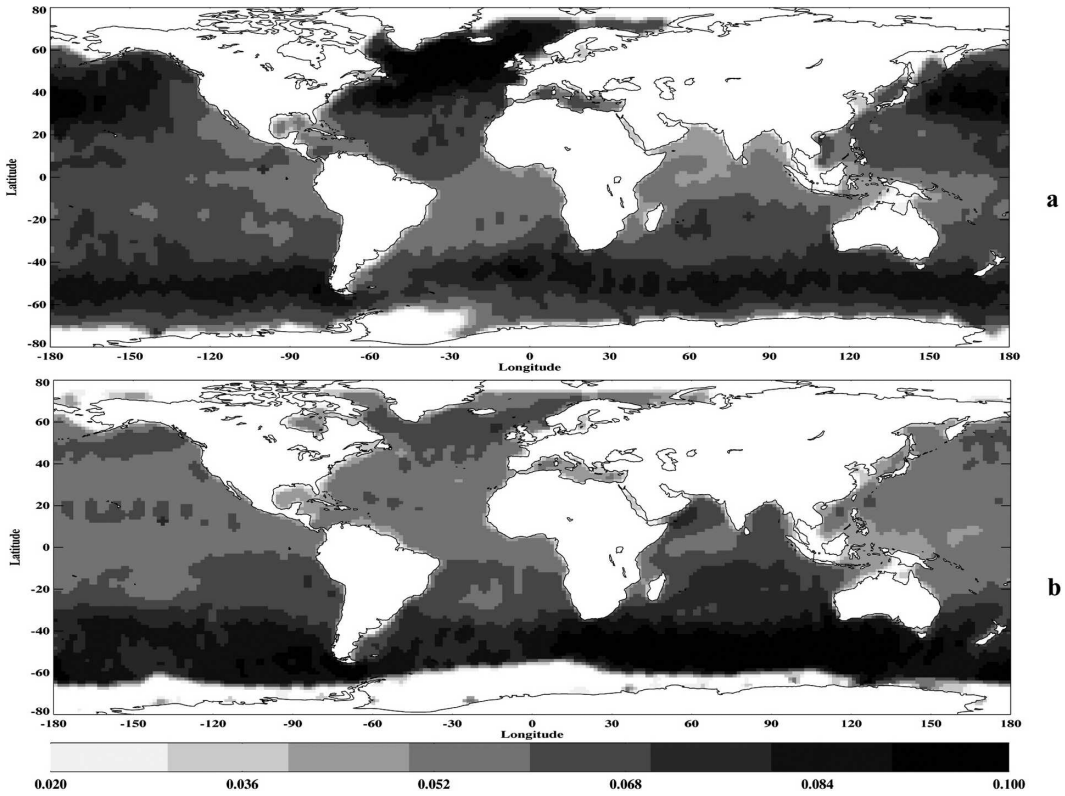

FIG. 5. Geographical distribution of the standard deviations of epoch retrieved with MLE-L for (a) cycle 13 and (b) cycle 19. Units: ns.

weighting is uniform, WLS basically reduces to least squares. This is what is chosen for the ESA processing of RA-2 (O. Z. Zanife 2006, personal communication; Zanife et al. 2003), even though the scheme continues to be referred to (confusingly, inconsistently, and erroneously) as "WLS" or "MLE."

Other retracker schemes have been developed also for other altimeters, most recently for that onboard *Jason-1*, for which special care had to be taken to account for occasional large mispointing errors (Thibaut et al. 2004a). Callahan and Rodríguez (2004) proposed another retracking scheme, sometimes referred to as singular value decomposition (SVD), which differs in many important respects from the ESA/Collecte Localisation Satellites (CLS) scheme but ultimately reduces to another implementation of unweighted least squares. Table 1 summarizes these particular characteristics of various retrackers mentioned in the literature and which are used later to discuss our results.

e. Ocean geophysical parameters

1) SIGNIFICANT WAVE HEIGHT

The determination of significant wave height is based on the assumption that the form of the radar return is given by the Brown (1977) or the Hayne (1980) model. The retrieval of nonlinear parameters will effect the estimation of SWH. Figure 1 shows two transmitted pulses for two different wave conditions. A higher slope of the leading edge is related to lower SWH (dark gray) and a lower slope to higher SWH (light gray). Altimeter SWH measurements (SGDR estimates) have been compared extensively with in situ measurements (e.g., buoys) and found to be highly reliable, with rms errors less than 0.3 m.

2) EPOCH (TIME ORIGIN)

The tracking point is a fixed reference point in the window used by the onboard tracking system to position the waveforms in the analysis window. The epoch corresponds to the half-power point on the leading edge of the waveform, which the onboard tracker aims to position at the tracking point. The retracker processes the averaged waveforms by fitting a theoretical waveform, which can return values of the epoch different to zero. This measures how much the tracker failed to position the echo correctly in the analysis window. This range offset, c*epoch/2, needs to be added to the information from the onboard tracker

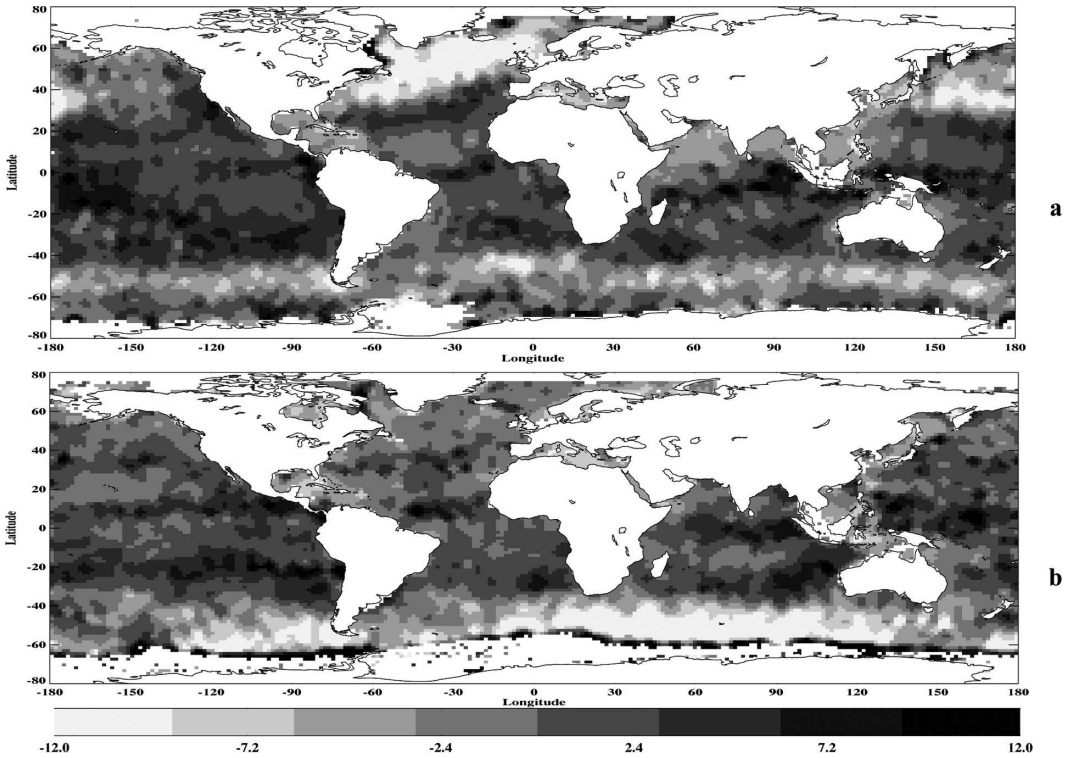

FIG. 6. Geographical distribution of the difference between SWH retrieved with MLE-L and RA-2 SGDR for (a) cycle 13 and (b) cycle 19. Units: cm.

for the estimation of the satellite to sea level distance.

3) WAVE SKEWNESS

The distribution of the surface elevation and slope has been traditionally established under the assumption of linear wave statistics (Gaussian distribution). Although this assumption is not strictly correct, it was the basis for the theory about the interaction of an altimeter radar return with the ocean surface (Brown 1977). The non-Gaussian distribution obtained under the weakly nonlinear wave statistics introduces additional nonlinear parameters and is based on Longuet-Higgins (1963) and Srokosz (1986). The skewness is the third-order moment of the ocean wave elevation distribution and is an indicator of the nonlinearity of ocean waves (characterized by peakier crests and flatter troughs).

There is little information in the literature about the estimation of wave skewness using theoretical and real averaged waveforms. Rodríguez and Chapman (1989) made some estimates using *Geosat* data. They obtained a standard deviation of 0.1 after averaging waveforms over 33 s, in order to reduce random noise. Using theoretical waveforms (with *ERS-1* radar specifications) and realistic noise characteristics, Tokmakian et al. (1994) found a standard deviation of 0.063 for 1-Hz data (after averaging 1000 theoretical individual echoes). More recently, using *Jason-1* data, Callahan and Rodríguez (2004) showed the geographical distribution of retracked wave skewness obtained by averaging over 31 s. They found values ranging between 0 and 0.1 and concluded that introducing a constant skewness in the retracker processing could generate regional and/or time-dependent errors in the estimation of sea surface height. Large values of skewness were found to be generally correlated with high SWH values, but the resulting skewness maps appear noisy with little apparent geographical coherence.

3. Altimeter datasets used

The 18-Hz averaged ocean waveforms selected for retracking and presented in this paper are from two complete RA-2 *Envisat* cycles corresponding to two different seasons: cycle 13 (13 January–17 February 2003) and cycle 19 (15 August–19 September 2003). The time-sampling interval in the Level 2 GDR products is 1.114 s (1 Hz), which corresponds to the mean of 20 averaged waveforms from the SGDR products (18 Hz). Hence, we present results of retracking waveforms es-

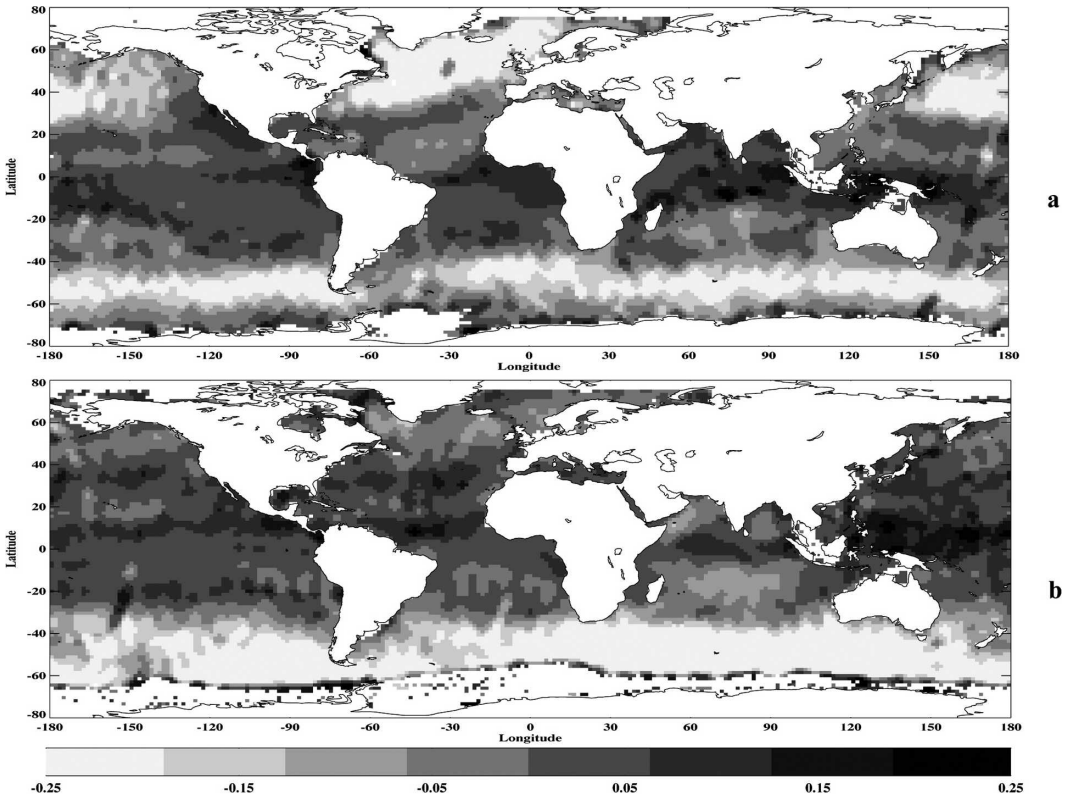

FIG. 7. Geographical distribution of the difference between epoch retrieved with MLE-L and RA-2 SGDR for (a) cycle 13 and (b) cycle 19. Units: ns.

timated by averaging packs of 20 averaged waveforms from SGDR products (18 Hz).

Unfortunately, it was not possible to make the conversion from the units of the RA-2 waveforms in the SGDR (FFT power units) to those used by the retracker (picowatts). To avoid this problem, the measured waveforms were scaled to arbitrary units between 0 and 1 prior to retracking. The cost of doing this is that the backscatter power values cannot be retrieved. We will therefore focus the comparison on the significant wave height and epoch obtained with the MLE retracker in linear and nonlinear modes, against the same parameters in the SGDR products retrieved with the ESA WLS ground processing.

4. Extraction of geophysical parameters from RA-2 waveforms

a. Results of MLE retracking in linear mode

1) SWH (LINEAR MODE)

Figures 2a and 2b show the geographical distribution of SWH (in meters) for cycle 13 (January–February 2003) and cycle 19 (August–September 2003), respectively, as obtained with the MLE retracking algorithm used in linear mode (MLE-L). The highest values (higher than 6 m) are mainly found in the Northern Hemisphere winter (Fig. 2a; Gulf Stream and Kuroshio areas) and the Southern Hemisphere winter (Fig. 2b; Antarctic Circumpolar Current area). In the Northern Hemisphere summer (Fig. 2b), the wave height in the Gulf Stream and Kuroshio Current areas is much lower with respect to their winter values (Fig. 2a). Note in the Indian Ocean the increased wave height due to the monsoon.

Figure 3 shows the standard deviation of SWH (in centimeters) for both cycles obtained from the MLE-L error estimates. The estimated errors range between 1.5 and 3.0 cm, indicating a high confidence in the retrieved SWH. The geographical distribution shows that the lowest and the highest standard deviations correspond to the lower and the higher values of SWH. This fact suggests that the slope of the leading edge may affect the uncertainties in the estimation of SWH, since a lower slope of the leading edge (higher wave heights) means a higher uncertainty (higher standard deviation) in the estimation of the parameter. This is somehow contradictory with the fact that for higher wave heights the leading edge is defined by a higher number of points with respect to lower wave heights (Fig. 1), but it

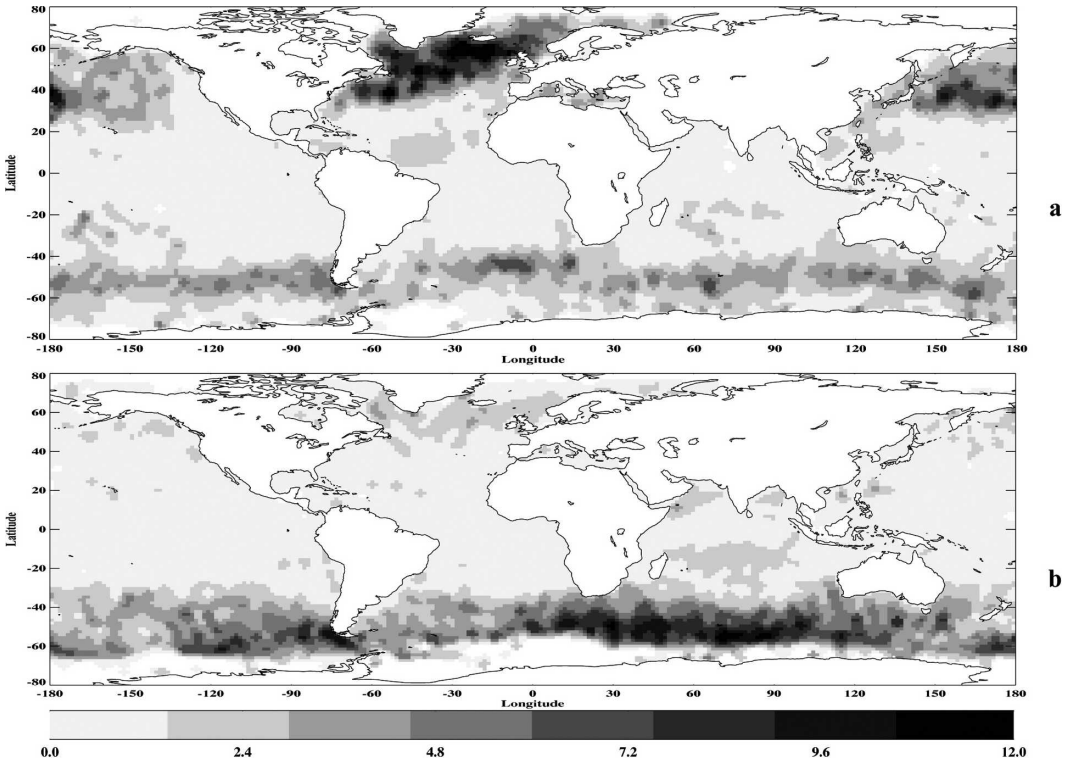

FIG. 8. Geographical distribution of the difference between SWH obtained with MLE-L and MLE-NL for (a) cycle 13 and (b) cycle 19. Units: cm.

could simply be that SWH variance increases with SWH (Carter and Tucker 1986).

2) EPOCH (LINEAR MODE)

The geographical distribution of epoch (in nanoseconds) retrieved with MLE-L is shown in Figs. 4a (cycle 13) and 4b (cycle 19). There is a clear correspondence between the location of the highest and the lowest values of wave height and epoch. The maximum magnitude obtained (up to 10.0 ns) in the areas of higher SWH (both cycles) demonstrates that the epoch obtained by retracking with MLE-L differs from the epoch of the averaged waveforms (initially set to zero) by more than three gates, producing a correction of up to 150 cm, which has to be added to the *range*.

Figures 5 shows the distribution of the standard deviation of the epoch estimates for both cycles. The range of values is [0.02, 0.10] (ns). Once again, the lowest (highest) values of epoch correspond to the lowest (highest) standard deviations.

3) COMPARISON BETWEEN SGDR PRODUCT AND MLE-L

The geographical distribution of the difference (in centimeters) between the SWH obtained with MLE-L and the SGDR product is shown in Figs. 6a (cycle 13) and 6b (cycle 19). The differences range between −12.0 and 12.0 cm, which demonstrates that the results between the two retrackers are consistent for SWH. For the two cycles analyzed, the lowest (negative) difference coincides with areas of high SWH, where the SWH obtained with MLE-L is larger than the SGDR estimates. In low-SWH zones, the differences are positive, except in the case of very low wave heights (SWH < 1 m), where MLE-L also produces larger estimates of SWH. We will discuss this later on, in the last section.

Figure 7 shows the distribution of the differences (in nanoseconds) between the epoch obtained with MLE-L and the SGDR product. The difference ranges between −0.25 and 0.25 ns, equivalent to [−3.75, 3.75] (cm) differences in range, and shows a consistency in the retrieval of the epoch with both retrackers. The lowest and highest differences are found in those zones with highest and lowest values of epoch, where MLE-L produces, respectively, larger and smaller estimates of epoch than SGDR.

All these results were obtained with a tracking point (TP) equal to 45. Earlier processing based on the nominal tracking point value of 46 resulted in an overall mean bias around 3.0 ns between the MLE-L results

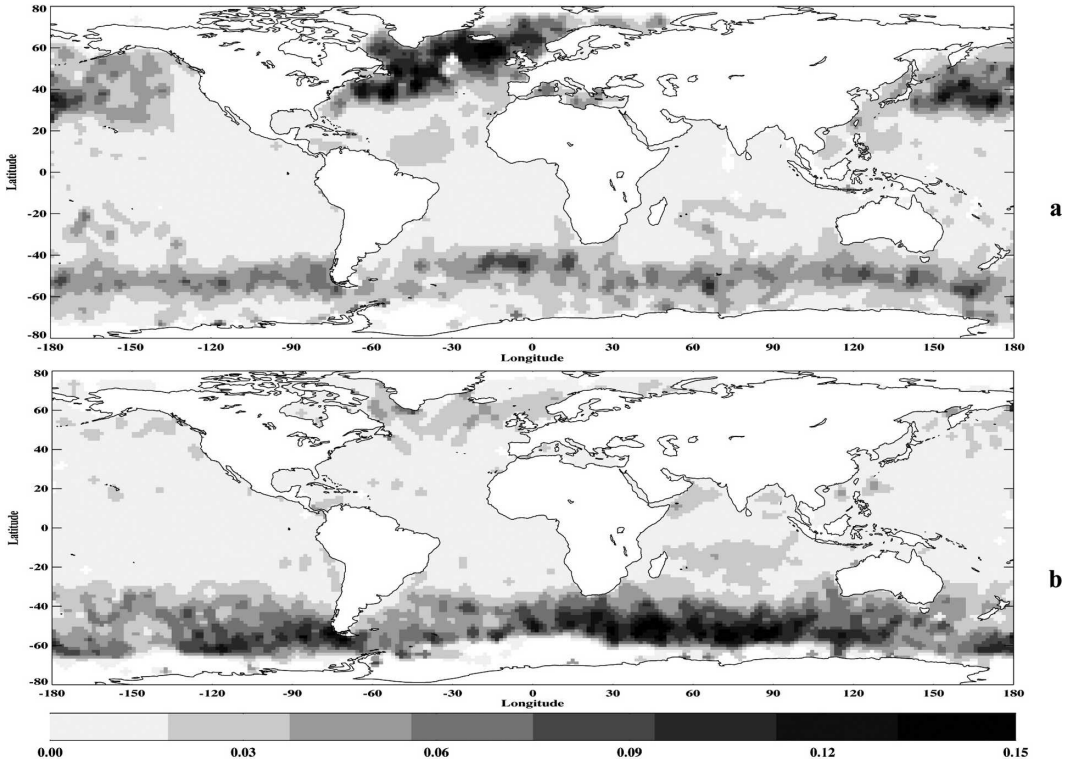

FIG. 9. Geographical distribution of the difference between epoch obtained with MLE-L and MLE-NL for (a) cycle 13 and (b) cycle 19. Units: ns.

and the SGDR records, leading us to repeat the analyses with TP = 45. Another unexpected feature of the SGDR processing that recently emerged is that the ESA retracker uses a value of σ_p equal to 0.53* (pulse width) instead of the nominal 0.425* (pulse width) (see section 2a for details). This difference, which until now was not publicized outside ESA and CLS, makes it difficult to draw any further conclusions from our comparisons between MLE-L and SGDR.

b. Results of MLE retracking in nonlinear mode

The geographical distribution of SWH and epoch obtained with the MLE retracker in nonlinear mode (MLE-NL) are similar to those obtained with MLE-L, so we only show the differences between the different retrackers, in order to investigate the effect of the retrieval of wave skewness on the estimation of the other parameters.

1) SWH (NONLINEAR MODE)

Figure 8 shows the differences for SWH obtained with MLE-L and MLE-NL for cycles 13 and 19. The difference ranges between 0 and 15.0 cm. MLE-NL seems to produce smaller values of SWH (positive differences) with respect to MLE-L. The magnitude of the differences is high in areas of high SWH (e.g., the Gulf Stream and Kuroshio in cycle 13 and the Antarctic Circumpolar Current in both cycles).

2) EPOCH (NONLINEAR MODE)

Figure 9 represents the distribution of the difference in epoch obtained with MLE-L and MLE-NL for cycles 13 and 19. The difference between MLE-L and MLE-NL is always positive, with MLE-NL producing smaller values of epoch than MLE-L [epoch (linear) > epoch (nonlinear)]. The biggest differences are found in areas such as the Gulf Stream and Kuroshio region (cycle 13) and the Antarctic Circumpolar Current (both cycles), showing the same geographical distribution as the SWH difference (Fig. 8).

3) WAVE SKEWNESS

We present in Fig. 10 the global maps of wave skewness as retrieved with MLE-NL for RA-2 in cycles 13 and 19. These results were obtained by adopting a numerical scheme, which forces retrieved skewness to be positive by fitting a new variable defined as the square root of skewness, $\lambda_{\text{sqrt}} = \lambda^{1/2}$. In this scheme, MLE re-

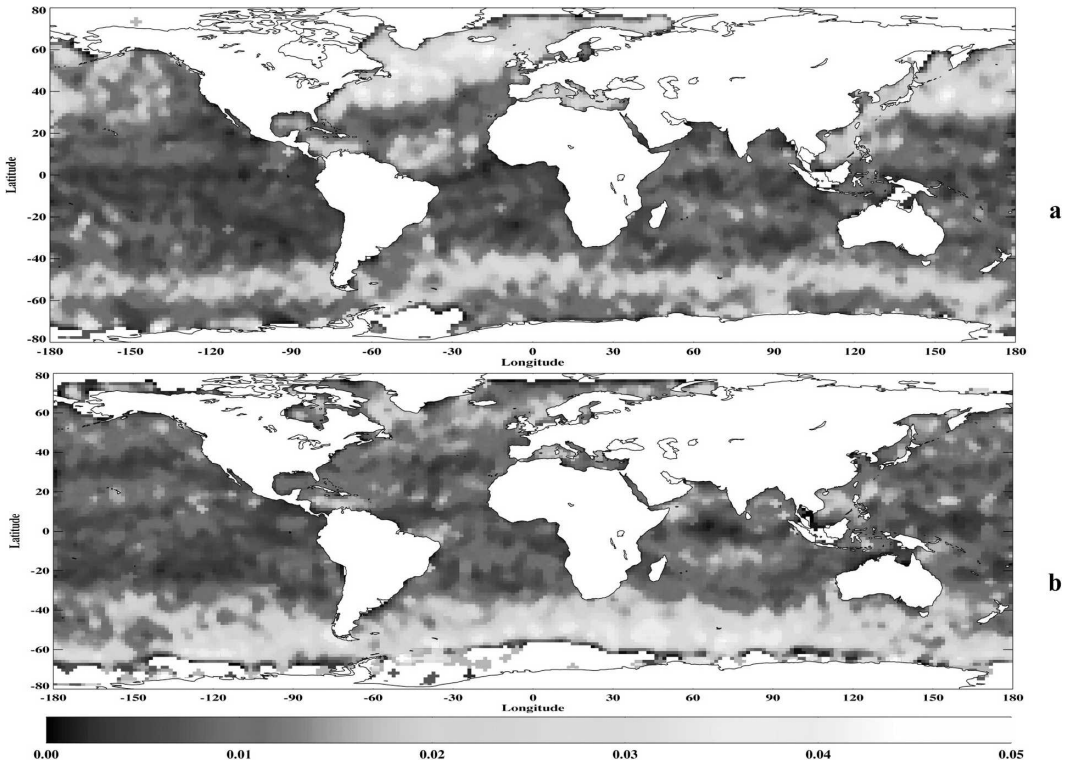

FIG. 10. Geographical distribution of wave skewness retrieved with MLE-NL for (a) cycle 13 and (b) cycle 19, with skewness constrained to positive-only values through a squared root skewness numerical retrieval scheme.

trieves λ_{sqrt} using information on the derivatives of λ_{sqrt}. Once λ_{sqrt} is retrieved, the result is squared to obtain the (now always positive) skewness. Values of skewness range between 0 and 0.05, with a large occurrence of skewness values close to zero. As expected, the distribution of skewness shows high (low) values in areas of high (low) wave height and epoch. These results are quantitatively consistent with those obtained by Callahan and Rodríguez (2004) for *Jason-1* data but show a much clearer (and physically more consistent) geographical coherence of the skewness of ocean waves.

All values of skewness shown in Fig. 10 are positive, but earlier analyses (where the retrieval scheme does not force skewness to be positive) had resulted in many occurrences of strongly negative skewness values (Fig. 11). Negative values of skewness are possible from a computational point of view but are difficult to justify physically. Large negative and positive skewness values were reported also by Thibaut et al. (2004b) for *Jason-1*, although their definition of the skewness pertains to the pdf of the range rather than the pdf of the heights (as is the case here). They estimated global and regional wave-skewness coefficients and concluded that a constant skewness value of –0.1 should be introduced in the ground retracking. A possible explanation for these large negative skewness results linked to using inaccurate attitude as input to the retracker is examined in another paper (GOM).

5. Discussion and conclusions

In this work, we applied an MLE-based ocean retracker scheme implemented at the National Oceanography Centre, Southampton, to *Envisat* RA-2 waveforms. Ocean geophysical parameters were retrieved under both linear and nonlinear ocean wave statistics assumptions using 18-Hz averaged ocean waveforms averaged to 1 Hz for two complete RA-2 *Envisat* cycles corresponding to two different seasons (Northern Hemisphere summer and winter). We compared our results with the outputs of the ESA "WLS" (effectively a least squares scheme; see section 2d) ground-based retracker contained in the RA-2 Level 2 SGDR products. Significant wave height and epoch (time origin) were retrieved with the MLE scheme in both linear and nonlinear mode, while the MLE scheme run in nonlinear mode provided the first estimates of global ocean wave skewness based on RA-2 *Envisat* averaged waveforms. From these results, we conclude the following.

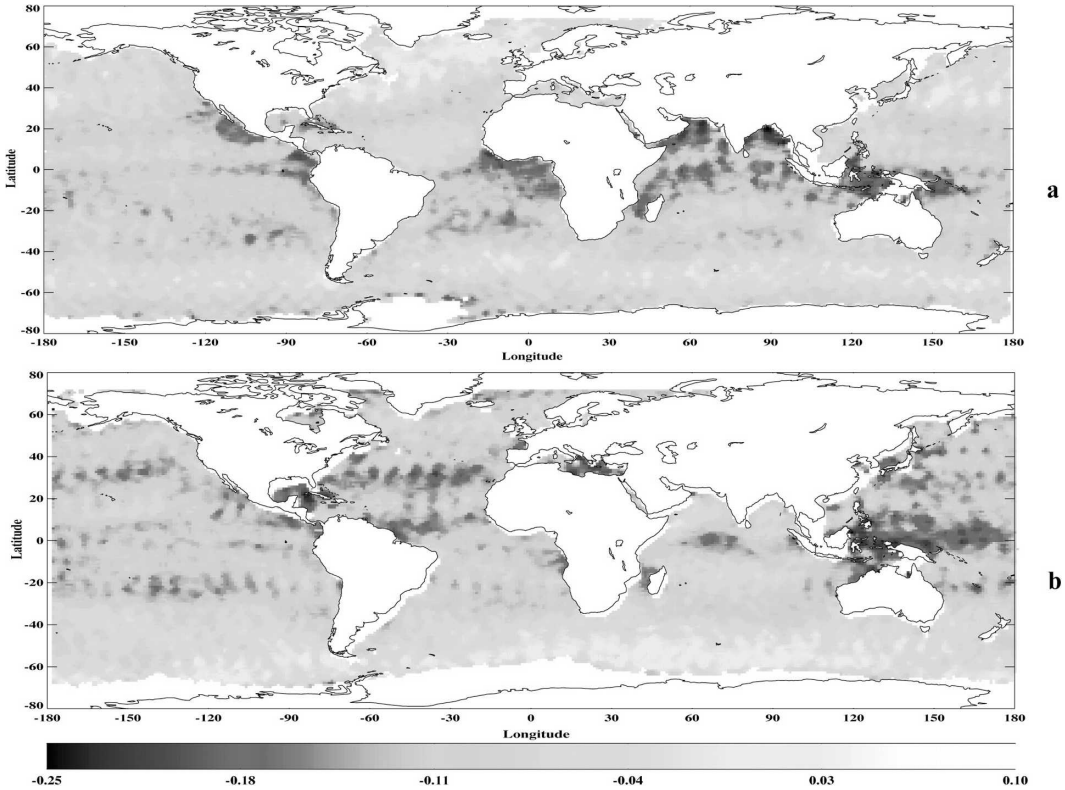

FIG. 11. Geographical distribution of wave skewness retrieved with MLE-NL for (a) cycle 13 and (b) cycle 19, without positive-only numerical retrieval scheme.

There is a direct relation between the geographical distributions of SWH and epoch, with large (small) SWH being matched by large (small) values of epoch. In low-wave-height conditions, the epoch obtained from the fitted waveform is close to zero, while for high SWH (up to 6 m) the epoch can be as large as 10 ns, which leads to a correction of the *range* of about 150 cm with respect to the nominal tracking point (45). The accuracy in the estimation of the range is particularly important for oceanographic applications, which require centimeter accuracy to derive information on geostrophic currents. More details about the exploitation of these results to estimate the role of skewness in altimeter tracker bias are given in a companion paper (GOM).

The comparison of geophysical parameters retrieved with MLE-linear (MLE-L) against the ESA SGDR output shows the two retracking schemes to be broadly consistent. However, our analyses also highlighted a number of unexplained discrepancies, and this work helped to bring to light certain aspects of the implementation of the ESA retracker that were previously not publicly known (e.g., "WLS" or "MLE" with uniform weights, different value of σ_p from nominal value, different tracking point, thermal noise not retrieved). These all have significant impacts on the results of the retracker and therefore make it impossible to draw any further conclusions from the comparisons between our MLE retracker and the "WLS" SGDR results.

The comparison between the MLE-L and MLE-nonlinear (MLE-NL) schemes demonstrated that MLE-L produces larger values of SWH and epoch than MLE-NL. Hence, accounting for nonlinear ocean wave effects results in a higher sea level estimate (closer to the altimeter), which is consistent with the negative range correction usually associated with sea-state bias. Quantitatively, the retrieval of skewness with MLE-NL affects SWH by about 2.7 cm (rms of the SWH differences between both retrackers for each cycle) and epoch by about 0.04 ns. For high-wave-height conditions (SWH $>$ 5 m) the impact of the retrieval of skewness on SWH is more important, with an rms difference of about 8.4 cm and 0.06 ns for epoch.

Our first attempts at estimating skewness with MLE-NL resulted in the frequent occurrence of large negative values of skewness, which, despite being possible computationally, have no physical meaning. We addressed this by adopting a numerical scheme, which forces retrieved skewness to be positive (essentially by fitting a new variable defined as the square root skew-

ness). This outcome is, however, somewhat unsatisfactory, and possible origins of these large negative skewness values are investigated in another paper (GOM) to look at the role of the Hamming windowing (which may violate the assumption of statistical independence between successive gates) and of using erroneous mispointing as input to the retracker. However, our analyses do indicate that credible global fields of skewness, with physically meaningful geographical coherence, may be extracted from *Envisat* RA-2 waveforms.

Acknowledgments. We thank the two anonymous referees for their input and comments, which helped to put this work in its proper context. This work has been done under the auspices of the European Space Agency in the framework of the Postdoctoral Research Fellowship Programme. Pierre Femenias (ESRIN-ESA) supplied the SGDR records used in this work under a Category-1 Project lead by Graham Quartly (NOCS). The authors want to thanks María Pilar Milagro-Pérez (ESRIN-ESA) for all the technical information she provided and the clarifications about the ESA WLS processing scheme and the RA-2 SGDR products.

REFERENCES

Abramowitz, M., and I. A. Stegun, 1968: Bessel functions of integer order. *Handbook of Mathematical Functions,* M. Abramowitz and I. A. Stegun, Eds., Dover, 374 pp.

Amarouche, L., P. Thibaut, O. Z. Zanife, J. P. Dumont, P. Vincent, and N. Steunou, 2004: Improving the Jason-1 ground retracking to better account for attitude effects. *Mar. Geodesy,* **27,** 171–197.

Barrick, D. E., and B. J. Lipa, 1985: Analysis and interpretation of altimeter sea echo. *Advances in Geophysics,* Vol. 27, Academic Press, 61–100.

Brown, G. S., 1977: The average impulse response of a rough surface and its applications. *IEEE J. Oceanic Eng.,* **2,** 67–74.

Callahan, P. S., and E. Rodríguez, 2004: Retracking Jason-1 data. *Mar. Geodesy,* **27,** 391–407.

Carter, D. J. T., and M. J. Tucker, 1986: Uncertainties in environmental design criteria. *Underwater Technol.,* **12,** 28–33.

Challenor, P. G., and M. A. Srokosz, 1989: The extraction of geophysical parameters from radar altimeter return from a non-linear sea surface. *Mathematics in Remote Sensing,* S. R. Brooks, Ed., Clarendon Press, 257–268.

Cox, D. R., and D. V. Hinkley, 1974: *Theoretical Statistics.* Chapman and Hall, 511 pp.

ESA, 2004: ENVISAT RA2/MWR product handbook. Issue 1.2. [Available online at http://envisat.esa.int/dataproducts/ra2-mwr/.]

Gomez-Enri, J., C. Gommenginger, M. Srokosz, P. Challenor, and M. Drinkwater, 2006: Envisat radar altimeter tracker bias. *Mar. Geodesy,* **29,** 19–38.

——, M. Srokosz, C. Gommenginger, P. Challenor, and M. Milagro-Perez, 2007: On the impact of mispointing error and Hamming filtering on altimeter waveform retracking and skewness retrieval. *Mar. Geodesy,* in press.

Griffiths, H. D., D. J. Wingham, P. G. Challenor, T. H. Guymer, and M. A. Srokosz, 1987: A study of mode switching and fast-delivery product algorithms for the ERS-1 altimeter. ESA Contract Rep. 6375/85/NL/BI, 250 pp.

Hayne, G. S., 1980: Radar altimeter mean return waveform from near-normal incidence ocean surface scattering. *IEEE Trans. Antennas Propag.,* **28,** 687–692.

Longuet-Higgins, M. S., 1963: The effect of nonlinearities on statistical distributions in the theory of sea waves. *J. Fluid Mech.,* **17,** 459–480.

Losquadro, G., 1983: Relationship between engineering and geophysical parameters. *ERS-1* Selenia Spazio Doc., Selenia Spazio, 350 pp.

Press, W. H., B. P. Flannery, S. A. Teukolsky, and W. T. Vetterling, 1988: *Numerical Recipes in C: The Art of Scientific Computing.* Cambridge University Press, 768 pp.

Rodríguez, E., 1988: Altimetry for non-Gaussian oceans: Height biases and estimation parameters. *J. Geophys. Res.,* **93,** 14 107–14 120.

——, and B. Chapman, 1989: Extracting ocean surface information from altimeter returns: The deconvolution method. *J. Geophys. Res.,* **94,** 9761–9778.

Srokosz, M. A., 1986: On the joint distribution of surface elevation and slopes for a nonlinear random sea, with an application to radar altimetry. *J. Geophys. Res.,* **91,** 995–1006.

Thibaut, P., L. Amarouche, O. Z. Zanife, N. Steunou, P. Vincent, and P. Raizonville, 2004a: Jason-1 altimeter ground processing look-up correction tables. *Mar. Geodesy,* **27,** 409–431.

——, ——, ——, and P. Vincent, 2004b: Estimation of the skewness coefficient in *Jason-1* altimeter data. *Proc. Ocean Surface Topography Science Team Meeting,* St. Petersburg, FL, CNES/NASA, CD-ROM.

Tokmakian, R. T., P. G. Challenor, H. Guymer, and M. A. Srokosz, 1994: The U.K. EODC ERS-1 altimeter oceans processing scheme. *Int. J. Remote Sens.,* **15,** 939–962.

Ulaby, F. T., R. K. Moore, and A. K. Fung, 1982:. *Radar Remote Sensing and Surface Scattering and Emission Theory.* Vol. II, *Microwave Remote Sensing: Active and Passive,* Addison-Wesley, 608 pp.

Zanife, O. Z., P. Vincent, L. Amarouche, J. P. Dumont, P. Thibaut, and S. Labroue, 2003: Comparison of the Ku-band range noise and the relative sea state bias of the Jason-1, TOPEX and POSEIDON-1 radar altimeters. *Mar. Geodesy,* **26,** 201–238.